Letter | Editors' Suggestion

Magnon-polaron driven thermal Hall effect in a Heisenberg-Kitaev antiferromagnet

N. Li,[1,*] R. R. Neumann,[2,*] S. K. Guang,[1,*] Q. Huang,[3] J. Liu,[3] K. Xia,[1] X. Y. Yue,[4] Y. Sun,[4] Y. Y. Wang,[4] Q. J. Li,[5] Y. Jiang,[5] J. Fang,[6] Z. Jiang,[6] X. Zhao,[7] A. Mook,[8] J. Henk,[2] I. Mertig,[2,†] H. D. Zhou,[3,‡] and X. F. Sun[1,4,§]

[1]Department of Physics, Hefei National Laboratory for Physical Sciences at Microscale, and Key Laboratory of Strongly-Coupled Quantum Matter Physics (CAS), University of Science and Technology of China, Hefei, Anhui 230026, People's Republic of China
[2]Institute of Physics, Martin Luther University Halle-Wittenberg, Halle (Saale) D-06120, Germany
[3]Department of Physics and Astronomy, University of Tennessee, Knoxville, Tennessee 37996-1200, USA
[4]Institute of Physical Science and Information Technology, Anhui University, Hefei, Anhui 230601, People's Republic of China
[5]School of Physics and Optoelectronics, Anhui University, Hefei, Anhui 230601, People's Republic of China
[6]School of Physics, Georgia Institute of Technology, Atlanta, Georgia 30332, USA
[7]School of Physical Sciences, University of Science and Technology of China, Hefei, Anhui 230026, People's Republic of China
[8]Institute of Physics, Johannes Gutenberg University, Mainz D-55128, Germany

(Received 28 February 2023; revised 23 August 2023; accepted 7 September 2023; published 4 October 2023)

We investigate the thermal Hall effect in the Heisenberg-Kitaev antiferromagnet $Na_2Co_2TeO_6$, where we observe negative thermal Hall conductivity (THC) with thermal Hall angles up to 2% at low magnetic fields, which changes the sign to positive THC at higher fields. Our theoretical calculations, incorporating spin-lattice coupling, reveal that the quantum-geometric Berry curvature of magnon polarons counteracts the purely magnonic contribution, resulting in a reversed sign and an increased magnitude in THC. This finding emphasizes the significance of spin-lattice coupling in understanding the thermal Hall effect.

DOI: 10.1103/PhysRevB.108.L140402

Topological phases of matter have received enormous attention in solid-state physics not only for their exceptional fundamental properties, but also for their potential technological impact. For example, topological band insulators feature protected, dissipationless edge channels [1–3], and topological order in strongly correlated electron systems (e.g., quantum spin liquids [4–6]) may be a route to fault-tolerant quantum computing [7,8]. Harvesting the potential of these exotic phases requires a reliable technique for their detection and characterization. An important probe for topological phases in insulators is the thermal Hall effect (THE), which denotes a transverse heat current response to a longitudinal temperature gradient [9,10]. Its *intrinsic* contribution is an invaluable probe of the Berry curvature, that is, a quantum-geometric property acting on the inherent quasiparticles, e.g., Majorana fermions [11,12], triplons [13,14], photons [15,16], and magnons [17–23], like a fictitious magnetic field. However, the ubiquitous phonons (quanta of lattice vibrations) interact and potentially hybridize with the aforementioned quasiparticles due to spin-lattice coupling (SLC) [24–26]. The band inversions of these quasiparticle-phonon hybrids establish another source of Berry curvature that may even dominate the low-temperature THE because of the low acoustic phonon energies. Hence, a detailed understanding of SLC and its effects on intrinsic heat transport is required.

In this joint experimental and theoretical work, we report the thermal Hall conductivity (THC) κ_{xy} of the Kitaev spin-liquid candidate $Na_2Co_2TeO_6$ (NCTO), which has attracted considerable attention recently [27–42]. Our field- and temperature-dependent measurements reveal a negative THC for out-of-plane magnetic fields below 10 T and a positive THC above 10 T at low temperatures. We attribute this sign change to a field-driven magnetic phase transition. As we demonstrate theoretically, magnons fail to explain not only the overall sign of THC, but also its order of magnitude, as THC is underestimated by a factor of ten. By taking SLC into account, magnons and phonons form hybrid quasiparticles, i.e., magnon polarons. The Berry curvature at the resulting avoided crossing between the lowest magnon and the acoustic phonon band is of opposite sign compared to the low-energy magnon Berry curvature without SLC. Hence, we reproduce both the correct overall sign and the order of magnitude of the experimental THC. The sign reversal of THC due to the hybridization of phonons and magnons is one of our main findings and is visualized in Fig. 1. Our results indicate the pivotal role of SLC in thermal transport, which may be also relevant to the interpretation of THC in related Heisenberg-Kitaev magnets [43–45].

NCTO is composed of Co^{2+} ions, arranged in layers of honeycomb lattices, whose effective $S = 1/2$ spins order in antiferromagnetic (AFM) zigzag chains [cf. Fig. 2(a)]. Employing a three-thermometer setup [Fig. 2(b), cf. Supplemental Material Section I.D. [46]], we have measured the temperature dependence of the longitudinal thermal conductivity $\kappa_{xx}(T)$ of NCTO at zero magnetic field [Fig. 2(c)]. According to previous studies, NCTO enters a magnetically

*These authors contributed equally to this work.
†ingrid.mertig@physik.uni-halle.de
‡hzhou10@utk.edu
§xfsun@ahu.edu.cn

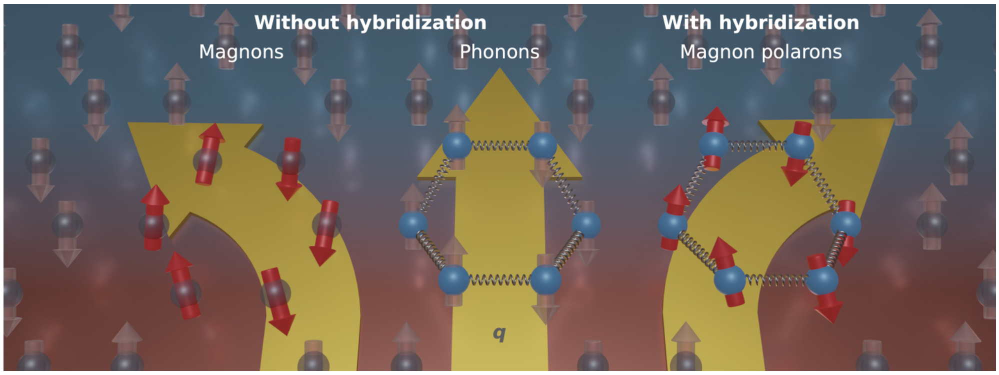

FIG. 1. Qualitative visualization of our theoretical results. Intrinsic thermal transport of distinct quasiparticles moving from hot to cold in a temperature gradient. Without hybridization, magnons contribute to the longitudinal and transversal transport, while phonons only contribute to the longitudinal one (in our approximation). With hybridization, magnons and phonons merge into magnon polarons and the transverse transport direction is reversed.

ordered state below the Néel temperature $T_N = 27$ K, followed by two possible spin reorientations around 16 K and 6 K, respectively [27–31]. Our $\kappa_{xx}(T)$ data show no obvious anomalies around 27 K and 16 K, in agreement with reported $\kappa_{xx}(T)$ data [47], but a slope change is noted below ∼6 K, possibly related to a spin reorientation [28,30]. At sub-Kelvin temperatures, $\kappa_{xx}(T)$ roughly follows a $T^{1.2}$ behavior, which is at variance with the T^3 or T^2 behavior expected for the phonon thermal conductivity at low temperatures in three or two dimensions, respectively [48]. Since magnons are frozen out at temperatures corresponding to energies below the spin-wave gap, their contribution does not explain the observed scaling law either. Therefore, this $T^{1.2}$ behavior may indicate the significance of interactions between phonons and magnons.

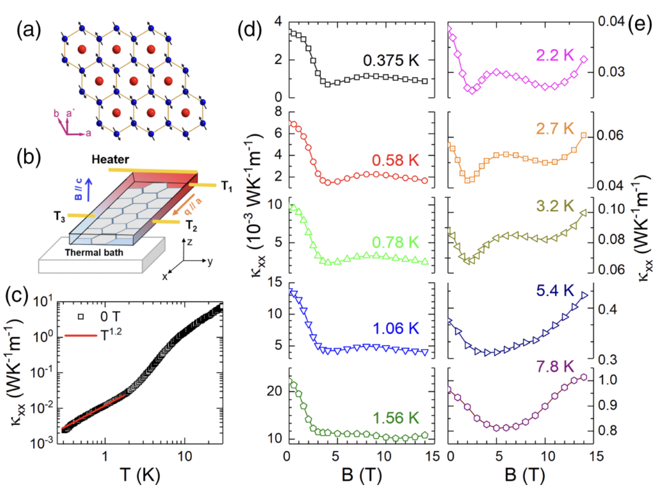

FIG. 2. Longitudinal thermal heat conductivity κ_{xx} of a $Na_2Co_2TeO_6$ single crystal. (a) Crystallographic spin structure of the *ab* plane of NCTO in the AFM state. The honeycomb lattice consists of cobalt ions (blue spheres) in the zigzag AFM arrangements (indicated by arrows), and the tellurium ions (red spheres) are located at the center of each honeycomb. The a^* axis is the in-plane direction perpendicular to the a axis. (b) Schematic of the experimental setup for the thermal Hall measurements. The heat current and the magnetic field are applied along the a and c axes, respectively. The longitudinal and transverse temperature gradients are determined by the difference between T_1 and T_2 and between T_2 and T_3, respectively. (c) Temperature dependence of the longitudinal thermal conductivity κ_{xx} at zero magnetic field. The zero-field data roughly display a $T^{1.2}$ behavior at very low temperatures, as the solid line indicates. (d) and (e) Magnetic-field dependence of the thermal conductivity at various temperatures and with $\boldsymbol{B} \parallel \boldsymbol{c}$.

The field dependence of $\kappa_{xx}(B)$ measured at various temperatures with $\boldsymbol{B} \parallel \boldsymbol{c}$ is depicted in Fig. 2(d) and 2(e). At $T < 1.56$ K, $\kappa_{xx}(B)$ decreases quickly with increasing field to reach a minimum around 4 T, and then shows a weak field dependence up to 14 T. At 2.2 K, 2.7 K, and 3.2 K, $\kappa_{xx}(B)$ manifests a double-valley structure, with valleys around 2 T and 10 T, respectively. At even higher temperatures, $\kappa_{xx}(B)$ exhibits a broad valley in the range of 5 to 10 T. Similar observations have been reported in Ref. [49].

Apart from the complex longitudinal thermal conductivity, we find a peculiar field dependence of the THC $\kappa_{xy}(B)$, which we have measured at various temperatures below T_N [cf. Figs. 3(a) and 3(b)]. At $T \leqslant 2.2$ K, with increasing field, $\kappa_{xy}(B)$ first exhibits a negative Hall response, reaching a minimum around 3 to 5 T, then it changes to a positive sign around 10 T and increases at higher fields. At 3.2 K and 5.4 K, $\kappa_{xy}(B)$ curves show a positive peak at low fields, followed by two zero crossings with increasing field. At 7.8 K, $\kappa_{xy}(B)$ is positive without sign reversal. We have plotted the temperature dependence of κ_{xy}/T at several fields in Fig. 3(c). It is evident that at $B = 3$ T and 5 T, with increasing temperature, κ_{xy} is negative and reaches a minimum around 2 K, and then changes to a positive sign around 3 K to 4 K. The thermal Hall angle κ_{xy}/κ_{xx} possesses a minimum around 4 T and changes to a positive sign around 10 T at temperatures below 2.2 K [cf. Fig. 3(d)]. The largest absolute value of κ_{xy}/κ_{xx} is around 2% at 0.78 K and 4 T.

In a magnetic insulator, the observed κ_{xy} may have several origins, including phonons, magnons, and fractionalized exotic quasiparticles such as spinons. In experiments on nonmagnetic insulators, the κ_{xy} of phonons does not exhibit a sign change [49,50], although this possibility cannot be ruled out here. For spinons, a nonzero κ_{xy} has only been observed in a quantum spin liquid with disordered spins [51–53]. Moreover, the 2% thermal Hall angle is exceptionally large for an

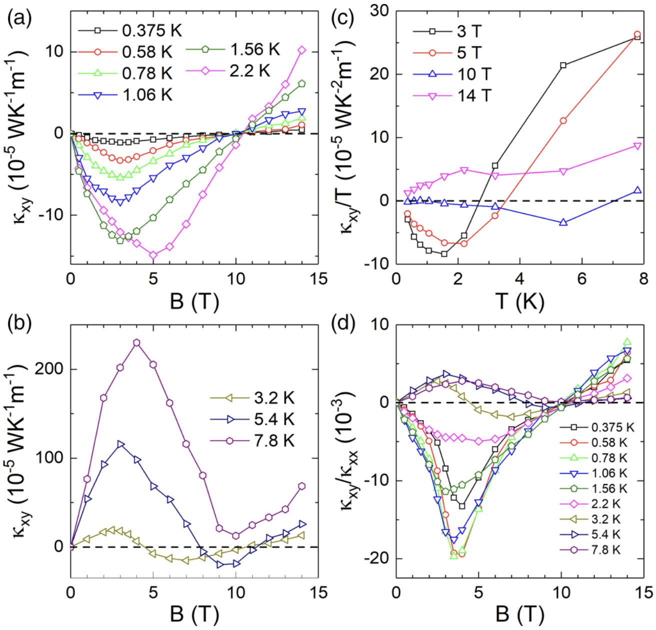

FIG. 3. Thermal Hall conductivity of a $Na_2Co_2TeO_6$ single crystal. (a) and (b) Field dependence of thermal Hall conductivity κ_{xy} for $\boldsymbol{B} \parallel \boldsymbol{c}$ at various temperatures. (c) Temperature dependence of κ_{xy}/T at selected magnetic fields. (d) Magnetic field dependence of the thermal Hall angle κ_{xy}/κ_{xx} at various temperatures.

insulator. The expected value, either originating from phonons or magnons, is typically around 0.3% to 0.6% or even lower [54], although similar thermal Hall angles have been observed in the insulating phases of the cuprate $Nd_{2-x}Ce_xCuO_4$ (up to 2%) [55], the iridate $Sr_2Ir_{1-x}Rh_xO_4$ (up to 3%) [56], and the pyrochlore magnet $Yb_2Ti_2O_7$ in its quantum spin-liquid state (up to 2%) [53].

The experimental results on the transverse transport properties of NCTO are subsequently explained by an effective, semiquantitative model. The starting point is the Heisenberg-Kitaev-Gamma-Gamma′ (HKGG′) Hamiltonian [57–59]

$$H = \frac{1}{2\hbar^2}\sum_{\langle ij\rangle_r} J_r \boldsymbol{S}_i \cdot \boldsymbol{S}_j + \frac{1}{2\hbar^2}\sum_{\langle ij\rangle}\big[K S_i^\gamma S_j^\gamma + \Gamma\big(S_i^\alpha S_j^\beta + S_i^\beta S_j^\alpha\big) + \Gamma'\big(S_i^\gamma S_j^\alpha + S_i^\gamma S_j^\beta + S_i^\alpha S_j^\gamma + S_i^\beta S_j^\gamma\big)\big]$$

that encompasses the Heisenberg exchange [J_r $(r = 1,\ 2,\ 3)$] up to third nearest neighbors, and the Kitaev (K), Gamma (Γ), Gamma′ (Γ') interactions between nearest neighbors. The magnetic field $\boldsymbol{B}$ enters via the Zeeman Hamiltonian

$$H_B = \frac{g\mu_B}{\hbar}\boldsymbol{B} \cdot \sum_i \boldsymbol{S}_i.$$

$\hbar$ denotes the reduced Planck constant, μ_B the Bohr magneton and g is the g-factor.

Here, we are interested in out-of-plane fields $\boldsymbol{B} \| \boldsymbol{c}$. Several parameter sets of the spin Hamiltonian have been determined for NCTO (Supplemental Material Table I [46]). In the following, we choose $J_1 = -3.2$ meV, $J_2 = 0.1$ meV, $J_3 = 1.2$ meV, $K = 2.7$ meV, $\Gamma = -2.9$ meV, $\Gamma' = 1.6$ meV, and $g = 2.3$ Refs. [34,36]. This parameter set (referred to as tc+) reproduces the critical fields in experimental reports on field-induced magnetic phase transitions (Supplemental Material Section II.C. [46]) and, as presented later, provides the best agreement with the experimental THC. Results for other parameter sets are reported in the Supplemental Material Section II.D. [46]. The weak interlayer coupling is neglected.

The antiferromagnetic ground state of the Hamiltonian at zero field is characterized by zigzag chains with intrachain ferromagnetic and interchain antiferromagnetic order. Applying a magnetic field cants the spins slightly, but they remain confined to the yz plane [cf. Fig. 4(a), left inset]. At the critical field of $B_{c1} = 10.8$ T the system passes a first-order phase transition into a spin-flop state, in which the spins lie within the zx plane [ferromagnetic component along z and Néel vector along x; cf. Fig. 4(a), right inset]. The magnetization saturates at $B_{c2} = 31.2$ T, at which the fully field-polarized phase is reached. These critical fields are supported by magnetometry measurements (Supplemental Material Section II.C. [46]).

The diagonalization of the linearized Hamiltonian yields the four magnon bands $\varepsilon_{n\boldsymbol{k}}$ $(n = 1,\ 2,\ 3,\ 4)$ [60,61]. Because of the spin-1/2 nature of the local magnetic moments, significant quantum fluctuations [62,63] are expected, which we discuss in the Supplemental Material Section II.F. [46]. The intrinsic contribution to THC is computed with the linear response formalism (cf. Supplemental Material Section II.D. [46]) [64].

Figure 4(a) shows κ_{xy} versus B_z as computed from free-magnon calculations for six temperatures. In the low-field phase, κ_{xy} is positive and changes sign at B_{c1} for all temperatures. This sign change is thus linked to the magnetic phase transition. However, the overall sign of κ_{xy} is at variance with the measured data [cf. Fig. 3(a)]. Attributed to the first-order transition, κ_{xy} is discontinuous at the phase transition, with the maximum left and the minimum right of B_{c1}. Moreover, the experimental data are underestimated by a factor of ten. Similar calculations with other parameter sets taken from the literature fail to reproduce the data as well (Supplemental Material Section II.D. [46]).

The foregoing suggests that magnons by themselves are not sufficient to explain the experimental data. It has been shown before that the hybridization of magnons and phonons can give rise to a thermal Hall effect [25,26,65–71]. We therefore consider out-of-plane oscillating phonons described by

$$H_{\mathrm{p}} = \sum_i \frac{\left(p_i^z\right)^2}{2M} + \frac{C}{4}\sum_{\langle ij\rangle}\left(u_i^z - u_j^z\right)^2,$$

where p_i^z is momentum and u_i^z is displacement, which are subject of a particular SLC arising from spin-orbit coupling [25,26,67,71–73],

$$H_{\mathrm{me}} = \frac{\tilde{\lambda}}{\hbar^2}\sum_i \sum_{\boldsymbol{\delta}} (\boldsymbol{S}_i \cdot \boldsymbol{\delta}) S_i^z \big(u_i^z - u_{i+\boldsymbol{\delta}}^z\big),$$

where $\boldsymbol{\delta}$ are the nearest-neighbor bond vectors for site. We neglect vibrations of nonmagnetic ions and other types of SLC for a minimal description. Furthermore, we consider a single acoustic phonon branch in the crystallographic Brillouin zone (that is, two branches in the magnetic Brillouin

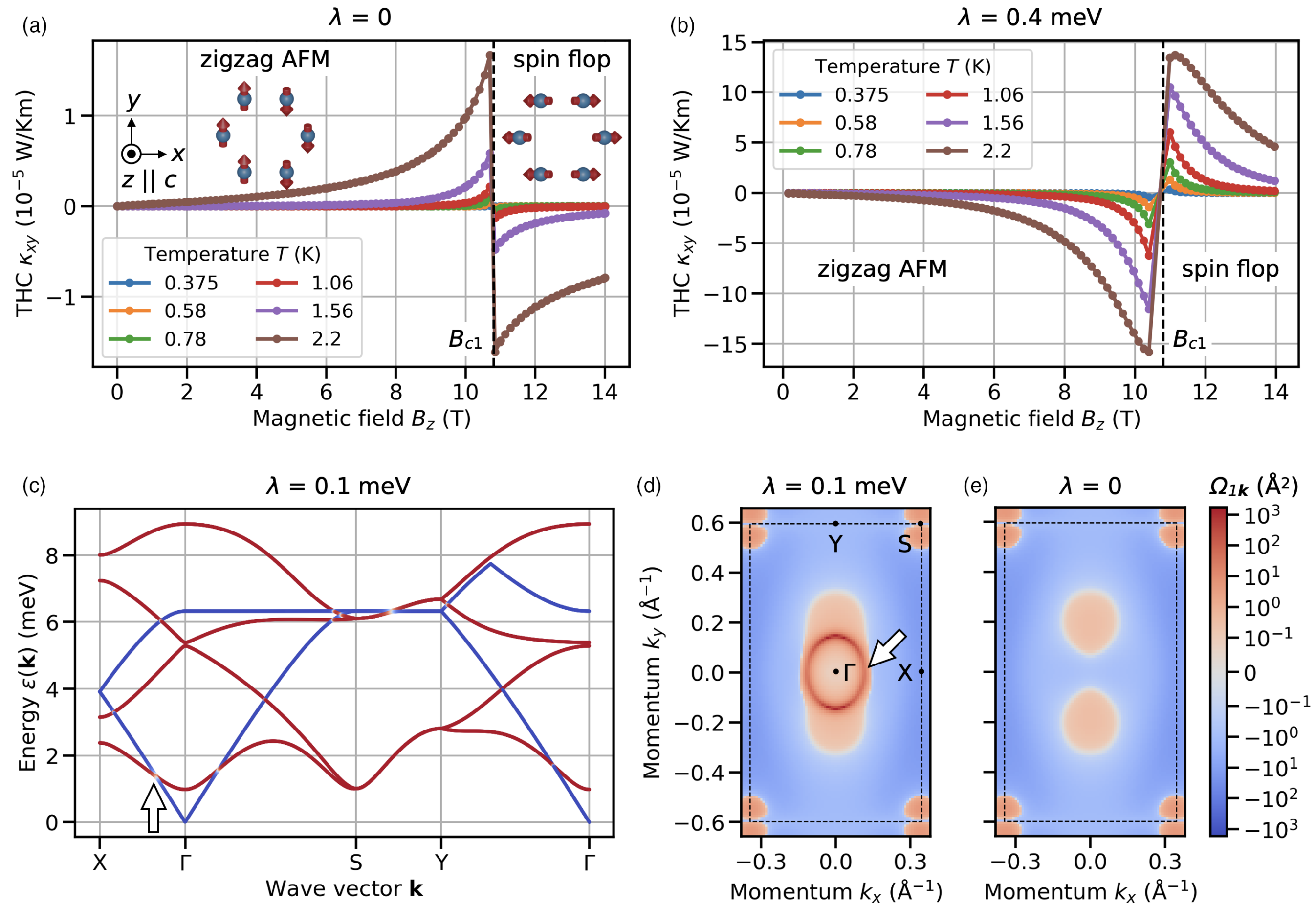

FIG. 4. Model calculations. (a) and (b) Thermal Hall conductivity κ_{xy} versus applied field B_z (a) without ($\lambda = 0\,\mathrm{meV}$) and (b) with ($\lambda = 0.4\,\mathrm{meV}$) SLC. Inset: Magnetic ground state of Co^{2+} ions in their two respective phases. (c) Magnon-polaron spectrum ε_{nk} along a high-symmetry path. Red, white, and blue color of the bands indicate the magnon, mixed, phonon character, respectively, of the modes; the magnetic field is 5 T. (d) and (e) Berry curvatures Ω_{nk} of the lowest bands $n = 1$ (d) with SLC ($\lambda = 0.1\,\mathrm{meV}$) and (e) without SLC ($\lambda = 0\,\mathrm{meV}$). Dashed rectangles in (d) and (e) mark the first Brillouin zone. The white arrows in (c) and (d) indicate the same avoided crossing. All results are obtained for the model of a two-dimensional honeycomb antiferromagnet with Heisenberg-Kitaev-Gamma-Gamma′ interactions ($J_1 = -3.2\,\mathrm{meV}$, $J_2 = 0.1\,\mathrm{meV}$, $J_3 = 1.2\,\mathrm{meV}$, $K = 2.7\,\mathrm{meV}$, $\Gamma = -2.9\,\mathrm{meV}$, $\Gamma' = 1.6\,\mathrm{meV}$, and $g = 2.3$) and coupling of the spins to out-of-plane lattice displacements (see text for further details).

zone). The relevant energy scale $\lambda = \tilde{\lambda} d_{\mathrm{nn}} \sqrt{\frac{\hbar}{2\sqrt{CM}}}$ [where M is the mass of Co^{2+} and $d_{\mathrm{nn}} = 3.0361$ Å is the (in-plane) nearest-neighbor distance] quantifies the strength of the SLC. The elastic constant C is chosen to yield a phonon velocity of 3000 m/s, which is supported by heat capacity measurements (Supplemental Material Section I.C. [46]) [74]. We proceed by bosonizing the spin and position operators, and extend the basis by the two phonon modes. The extended Hamiltonian is then diagonalized, and κ_{xy} is computed as before. The SLC strength $\lambda = 0.4\,\mathrm{meV}$ has been fitted as an effective parameter to reproduce the experimental THC at 2.2 K.

Figure 4(b) displays κ_{xy} versus B_z in the presence of SLC. Compared to exclusive magnon transport, the overall sign of κ_{xy} is reversed and the sign change at the magnetic phase transition remains intact. Furthermore, κ_{xy}'s order of magnitude has increased and matches that of the experimental data. In short, agreement with the experiment has increased significantly.

The sign change and the increase of $|\kappa_{xy}|$ are attributed to hybrid quasiparticles that we refer to as magnon polarons. These normal modes are superpositions of magnons and phonons. Their hybrid nature is prominent in the band structure with SLC [Fig. 4(c)] at avoided crossings: their character changes continuously from magnon-like (red) to phonon-like (blue). The avoided crossing between the acoustic phonon branch and the lower magnon band generates a positive Berry curvature in the lowest band, indicated by a white arrow in Fig. 4(d). This pronounced, low-energy Berry curvature dominates the transport and explains the negative sign in the zigzag antiferromagnetic phase. This finding is contrasted with the Berry curvature in the absence of SLC [Fig. 4(e)]. Ignoring the phonon bands [blue in Fig. 4(c)], the magnon bands exhibit a spin-wave gap, and their lowest energies are at the Γ and S points. The Berry curvature of the lowest magnon band [Fig. 4(e)] at these points is negative and positive, respectively. Since the two lower magnon bands are degenerate at S and the upper band exhibits the opposite Berry curvature at S, the Berry curvature at Γ mostly governs the thermal transport at low temperatures. This Berry curvature is, however, opposite to the emerging Berry curvature caused by the hybridization. Thus, there is a competition between pure magnon transport and magnon-polaron transport in the presence of SLC.

The gradual suppression and sign reversal of κ_{xy} by the coupling to phonons hold for lower temperatures. At higher temperatures, the magnon bands are strongly populated and the transport coefficient changes sign (Supplemental Material [46]). This competitive interplay between phonons and magnons is contrasted by the results of Zhang *et al.* [26] for the honeycomb ferromagnet VI_3, which has been modeled with the Dzyaloshinskii-Moriya interaction (DMI) as the source of the magnon Berry curvature. There, an amplification of THC was found due to the SLC. Notably, an attenuation can be found for reversed DMI, which produces the same magnon spectrum, but opposite Berry curvature; hence, both amplification and attenuation of THC are within the reach of the DMI model with SLC. In contrast, the HKGG′ model with SLC uniquely fixes both the sign of the magnon and the magnon-polaron Berry curvatures and, therefore, their relative sign. This renders the agreement between theory and experiment nontrivial. Overall, whether SLC leads to an amplification or an attenuation depends on the spin Hamiltonian and the particular form of SLC. Examples for the amplification by SLC in the HKGG′ model are reported in the Supplemental Material [46] with different parameters. A systematic study is needed to predict which of these two scenarios can be expected in other systems.

The model including SLC achieves an agreement between theoretical and experimental results in overall sign, magnitude, and the general field dependence, in contrast to the pure magnon calculations. The remaining quantitative disagreement between the effective theoretical model and experiment could be caused by the presence of multiple domains close to the phase transition, which is not accounted for in our model, the restriction to one phonon band and one particular type of SLC, and the disregard of vibrational degrees of freedom of nonmagnetic ions. The deviation between the minima of $\kappa_{xy}(B_z)$ measured at 3 T and computed at 10 T may be attributed to extrinsic contributions to THC, as indicated by the correlation between the measured minima of κ_{xx} and κ_{xy} at similar fields [cf. Figs. 2(d), 2(e), and 3(a)]. Hence, at lower fields, extrinsic contributions appear to be relevant for a better quantitative agreement, while at larger fields, due to the lack of a similar prominent correlation, their relevance might be limited. Therefore, the extrinsic contributions to THC such as magnon-phonon scattering, magnon-magnon scattering, and scattering of phonons or magnons at (magnetic) impurities should be investigated in a more comprehensive quantitative theory.

An open question for NCTO is whether its ground state is of zigzag antiferromagnetic or of triple-Q nature. While several studies have argued in favor of triple-Q [33,39,40], another reports inconsistent observations with the triple-Q ground state [41]. Our study shows that the zigzag antiferromagnetic ground state is compatible with THC measurements; however, we cannot conclusively rule out the possibility of a triple-Q ground state. In the triple-Q state, the noncollinear spin texture gives rise to a more complex SLC and magnon-phonon hybridization, leading to a larger set of adjustable parameters, which would have to be obtained from density functional theory. Whether the triple-Q ground state is also compatible with our THC measurements needs to be addressed in the future.

Finally, our results—in particular, the fact that magnon polarons and pure magnons can drive opposite heat currents of different magnitudes—demonstrate that SLC may completely alter the low-temperature transport properties and overshadow predicted transport signatures of isolated quasiparticles like topological magnons. Instead of transport signatures of isolated exotic spin excitations, a more unified approach that includes the hybridization with phonons is necessary for the interpretation of such transport experiments. To verify the importance of SLC in NCTO, but also more generally, an independent determination of the SLC by *ab initio* calculations or magnetoelastic experiments is required that should be combined with model calculations to quantify the impact on THC. In short, our results call for a systematic analysis of the role of SLC in THC.

We thank I. Kimchi for insightful discussions, and W. J. Chu and X. H. Zhou for their help with the experiments. This work was supported by the National Natural Science Foundation of China (Grants No. 12274388, No. 12174361, No. 12025408, No. 11904003, and No. 12274001) and the Nature Science Foundation of Anhui Province (Grants No. 1908085MA09, No. 2108085QA22, and No. 2208085MA09). The work at the University of Tennessee and Georgia Tech was supported by the U.S. Department of Energy (Awards No. DE-SC-0020254 and No. DE-FG02-07ER46451). A.M., J.H., and I.M. acknowledge funding from Deutsche Forschungsgemeinschaft (DFG, German Research Foundation) (Projects No. 504261060 and No. SFB TRR 227).

[1] K. v. Klitzing, G. Dorda, and M. Pepper, New method for high-accuracy determination of the fine-structure constant based on quantized Hall resistance, Phys. Rev. Lett. **45**, 494 (1980).

[2] D. J. Thouless, M. Kohmoto, M. P. Nightingale, and M. den Nijs, Quantized Hall conductance in a two-dimensional periodic potential, Phys. Rev. Lett. **49**, 405 (1982).

[3] F. D. M. Haldane, Model for a quantum Hall effect without Landau levels: Condensed-matter realization of the parity anomaly, Phys. Rev. Lett. **61**, 2015 (1988).

[4] P. W. Anderson, Resonating valence bonds: A new kind of insulator? Mater. Res. Bull. **8**, 153 (1973).

[5] R. Moessner and S. L. Sondhi, Resonating valence bond phase in the triangular lattice quantum dimer model, Phys. Rev. Lett. **86**, 1881 (2001).

[6] A. Kitaev, Anyons in an exactly solved model and beyond, Ann. Phys. **321**, 2 (2006).

[7] A. Stern and N. H. Lindner, Topological quantum computation: From basic concepts to first experiments, Science **339**, 1179 (2013).

[8] V. Lahtinen and J. Pachos, A short introduction to topological quantum computation, SciPost Physics **3**, 021 (2017).
[9] H. Katsura, N. Nagaosa, and P. A. Lee, Theory of the thermal Hall effect in quantum magnets, Phys. Rev. Lett. **104**, 066403 (2010).
[10] R. Matsumoto, R. Shindou, and S. Murakami, Thermal Hall effect of magnons in magnets with dipolar interaction, Phys. Rev. B **89**, 054420 (2014).
[11] J. Nasu, J. Yoshitake, and Y. Motome, Thermal transport in the Kitaev model, Phys. Rev. Lett. **119**, 127204 (2017).
[12] Y. Kasahara, T. Ohnishi, Y. Mizukami, O. Tanaka, S. Ma, K. Sugii, N. Kurita, H. Tanaka, J. Nasu, Y. Motome, T. Shibauchi, and Y. Matsuda, Majorana quantization and half-integer thermal quantum Hall effect in a Kitaev spin liquid, Nature (London) **559**, 227 (2018).
[13] J. Romhányi, K. Penc, and R. Ganesh, Hall effect of triplons in a dimerized quantum magnet, Nat. Commun. **6**, 6805 (2015).
[14] P. A. McClarty, F. Krüger, T. Guidi, S. F. Parker, K. Refson, A. W. Parker, D. Prabhakaran, and R. Coldea, Topological triplon modes and bound states in a Shastry–Sutherland magnet, Nat. Phys. **13**, 736 (2017).
[15] S. Raghu and F. D. M. Haldane, Analogs of quantum-Hall-effect edge states in photonic crystals, Phys. Rev. A **78**, 033834 (2008).
[16] L. Lu, J. D. Joannopoulos, and M. Soljačić, Topological photonics, Nat. Photon **8**, 821 (2014).
[17] Y. Onose, T. Ideue, H. Katsura, Y. Shiomi, N. Nagaosa, and Y. Tokura, Observation of the magnon Hall effect, Science, **329**, 297 (2010).
[18] T. Ideue, Y. Onose, H. Katsura, Y. Shiomi, S. Ishiwata, N. Nagaosa, and Y. Tokura, Effect of lattice geometry on magnon Hall effect in ferromagnetic insulators, Phys. Rev. B **85**, 134411 (2012).
[19] R. Shindou, R. Matsumoto, S. Murakami, and J. Ohe, Topological chiral magnonic edge mode in a magnonic crystal, Phys. Rev. B **87**, 174427 (2013).
[20] A. Mook, J. Henk, and I. Mertig, Magnon Hall effect and topology in kagome lattices: A theoretical investigation, Phys. Rev. B **89**, 134409 (2014).
[21] R. Chisnell, J. S. Helton, D. E. Freedman, D. K. Singh, R. I. Bewley, D. G. Nocera, and Y. S. Lee, Topological magnon bands in a kagome lattice ferromagnet, Phys. Rev. Lett. **115**, 147201 (2015).
[22] A. Mook, J. Henk, and I. Mertig, Thermal Hall effect in noncollinear coplanar insulating antiferromagnets, Phys. Rev. B **99**, 014427 (2019).
[23] R. R. Neumann, A. Mook, J. Henk, and I. Mertig, Thermal Hall effect of magnons in collinear antiferromagnetic insulators: Signatures of magnetic and topological phase transitions, Phys. Rev. Lett. **128**, 117201 (2022).
[24] R. Takahashi and N. Nagaosa, Berry curvature in magnon-phonon hybrid systems, Phys. Rev. Lett. **117**, 217205 (2016).
[25] S. Zhang, G. Go, K.- J. Lee, and S. K. Kim, SU(3) topology of magnon-phonon hybridization in 2D antiferromagnets, Phys. Rev. Lett. **124**, 147204 (2020).
[26] H. Zhang, C. Xu, C. Carnahan, M. Sretenovic, N. Suri, D. Xiao, and X. Ke, Anomalous thermal Hall effect in an insulating van der Waals magnet, Phys. Rev. Lett. **127**, 247202 (2021).
[27] L. Viciu, Q. Huang, E. Morosan, H. W. Zandbergen, N. I. Greenbaum, T. McQueen, and R. J. Cava, Structure and basic magnetic properties of the honeycomb lattice compounds $Na_2Co_2TeO_6$ and $Na_3Co_2SbO_6$, J. Solid State Chem. **180**, 1060 (2007).
[28] E. Lefrançois, M. Songvilay, J. Robert, G. Nataf, E. Jordan, L. Chaix, C. V. Colin, P. Lejay, A. Hadj-Azzem, R. Ballou, and V. Simonet, Magnetic properties of the honeycomb oxide $Na_2Co_2TeO_6$, Phys. Rev. B **94**, 214416 (2016).
[29] A. K. Bera, S. M. Yusuf, A. Kumar, and C. Ritter, Zigzag antiferromagnetic ground state with anisotropic correlation lengths in the quasi-two-dimensional honeycomb lattice compound $Na_2Co_2TeO_6$, Phys. Rev. B **95**, 094424 (2017).
[30] G. Xiao, Z. Xia, W. Zhang, X. Yue, S. Huang, X. Zhang, F. Yang, Y. Song, M. Wei, H. Deng, and D. Jiang, Crystal growth and the magnetic properties of $Na_2Co_2TeO_6$ with quasi-two-dimensional honeycomb lattice, Cryst. Growth Des. **19**, 2658 (2019).
[31] W. Yao and Y. Li, Ferrimagnetism and anisotropic phase tunability by magnetic fields in $Na_2Co_2TeO_6$, Phys. Rev. B **101**, 085120 (2020).
[32] M. Songvilay, J. Robert, S. Petit, J. A. Rodriguez-Rivera, W. D. Ratcliff, F. Damay, V. Balédent, M. Jiménez-Ruiz, P. Lejay, E. Pachoud, A. Hadj-Azzem, V. Simonet, and C. Stock, Kitaev interactions in the Co honeycomb antiferromagnets $Na_3Co_2SbO_6$ and $Na_2Co_2TeO_6$, Phys. Rev. B **102**, 224429 (2020).
[33] W. Chen, X. Li, Z. Hu, Z. Hu, L. Yue, R. Sutarto, F. He, K. Iida, K. Kamazawa, W. Yu, X. Lin, and Y. Li, Spin-orbit phase behavior of $Na_2Co_2TeO_6$ at low temperatures, Phys. Rev. B **103**, L180404 (2021).
[34] G. Lin *et al.*, Field-induced quantum spin disordered state in spin-1/2 honeycomb magnet $Na_2Co_2TeO_6$, Nat. Commun. **12**, 5559 (2021).
[35] C. Kim, J. Jeong, G. Lin, P. Park, T. Masuda, S. Asai, S. Itoh, H.- S. Kim, H. Zhou, J. Ma, and J.- G. Park, Antiferromagnetic Kitaev interaction in $J_{\mathrm{eff}} = 1/2$ cobalt honeycomb materials $Na_3Co_2SbO_6$ and $Na_2Co_2TeO_6$, J. Phys.: Condens. Matter **34**, 045802 (2021).
[36] A. M. Samarakoon, Q. Chen, H. Zhou, and V. O. Garlea, Static and dynamic magnetic properties of honeycomb lattice antiferromagnets $Na_2M_2TeO_6$, M = Co and Ni, Phys. Rev. B **104**, 184415 (2021).
[37] G. Xiao, Z. Xia, Y. Song, and L. Xiao, Magnetic properties and phase diagram of quasi-two-dimensional $Na_2Co_2TeO_6$ single crystal under high magnetic field, J. Phys.: Condens. Matter **34**, 075801 (2021).
[38] A. L. Sanders, R. A. Mole, J. Liu, A. J. Brown, D. Yu, C. D. Ling, and S. Rachel, Dominant Kitaev interactions in the honeycomb materials $Na_3Co_2SbO_6$ and $Na_2Co_2TeO_6$, Phys. Rev. B **106**, 014413 (2022).
[39] W. G. F. Krüger, W. Chen, X. Jin, Y. Li, and L. Janssen, Triple-Q order in $Na_2Co_2TeO_6$ from proximity to hidden-SU(2)-symmetric point, arXiv:2211.16957.
[40] W. Yao, Y. Zhao, Y. Qiu, C. Balz, J. R. Stewart, J. W. Lynn, and Y. Li, Magnetic ground state of the Kitaev $Na_2Co_2TeO_6$ spin liquid candidate, Phys. Rev. Res. **5**, L022045 (2023).
[41] S. Zhang, S. Lee, A. J. Woods, W. K. Peria, S. M. Thomas, R. Movshovich, E. Brosha, Q. Huang, H. Zhou, V. S. Zapf, and M. Lee, Electronic and magnetic phase diagrams of the Kitaev quantum spin liquid candidate $Na_2Co_2TeO_6$, Phys. Rev. B **108**, 064421 (2023).

[42] S. Guang, N. Li, Q. Huang, K. Xia, Y. Wang, H. Liang, Y. Sun, Q. Li, X. Zhao, R. L. Luo, G. Chen, H. Zhou, and X. Sun, Anisotropic in-plane heat transport of Kitaev magnet $Na_2Co_2TeO_6$, arXiv:2307.06316.

[43] Y. Singh, S. Manni, J. Reuther, T. Berlijn, R. Thomale, W. Ku, S. Trebst, and P. Gegenwart, Relevance of the Heisenberg-Kitaev model for the honeycomb lattice iridates A_2IrO_3, Phys. Rev. Lett. **108**, 127203 (2012).

[44] K. W. Plumb, J. P. Clancy, L. J. Sandilands, V. V. Shankar, Y. F. Hu, K. S. Burch, H.- Y. Kee, and Y.- J. Kim, α-$RuCl_3$: A spin-orbit assisted Mott insulator on a honeycomb lattice, Phys. Rev. B **90**, 041112 (2014).

[45] C. Wong, M. Avdeev, and C. D. Ling, Zig-zag magnetic ordering in honeycomb-layered $Na_3Co_2SbO_6$, J. Solid State Chem. **243**, 18 (2016).

[46] See Supplemental Material at http://link.aps.org/supplemental/10.1103/PhysRevB.108.L140402 for additional experimental results on magnetometry, heat capacity, and longitudinal thermal conductivity measurements as well as theoretical results on critical magnetic fields, thermal Hall conductivity with and without spin-lattice coupling, and spin fluctuations.

[47] X. Hong, M. Gillig, R. Hentrich, W. Yao, V. Kocsis, A. R. Witte, T. Schreiner, D. Baumann, N. Pérez, A. U. B. Wolter, Y. Li, B. Büchner, and C. Hess, Strongly scattered phonon heat transport of the candidate Kitaev material $Na_2Co_2TeO_6$, Phys. Rev. B **104**, 144426 (2021).

[48] R. Berman, *Thermal Conduction in Solids* (Clarendon Press, Oxford, 1976).

[49] S. K. Guang, N. Li, R. L. Luo, Q. Huang, Y. Y. Wang, X. Y. Yue, K. Xia, Q. J. Li, X. Zhao, G. Chen, H. D. Zhou, and X. F. Sun, Thermal transport of fractionalized antiferromagnetic and field induced states in the Kitaev material $Na_2Co_2TeO_6$, Phys. Rev. B **107**, 184423 (2023).

[50] C. Strohm, G. L. J. A. Rikken, and P. Wyder, Phenomenological evidence for the phonon Hall effect, Phys. Rev. Lett. **95**, 155901 (2005).

[51] H. Doki, M. Akazawa, H.- Y. Lee, J. H. Han, K. Sugii, M. Shimozawa, N. Kawashima, M. Oda, H. Yoshida, and M. Yamashita, Spin thermal Hall conductivity of a kagome antiferromagnet, Phys. Rev. Lett. **121**, 097203 (2018).

[52] M. Hirschberger, J. W. Krizan, R. J. Cava, and N. P. Ong, Large thermal Hall conductivity of neutral spin excitations in a frustrated quantum magnet, Science **348**, 106 (2015).

[53] M. Hirschberger, P. Czajka, S. M. Koohpayeh, W. Wang, and N. P. Ong, Enhanced thermal Hall conductivity below 1 Kelvin in the pyrochlore magnet $Yb_2Ti_2O_7$, arXiv:1903.00595.

[54] L. Chen, M.-E. Boulanger, Z.- C. Wang, F. Tafti, and L. Taillefer, Large phonon thermal Hall conductivity in the antiferromagnetic insulator Cu_3TeO_6, Proc. Natl. Acad. Sci. USA **119**, e2208016119 (2022).

[55] M.- E. Boulanger, G. Grissonnanche, É. Lefrançois, A. Gourgout, K.- J. Xu, Z.- X. Shen, R. L. Greene, and L. Taillefer, Thermal Hall conductivity of electron-doped cuprates, Phys. Rev. B **105**, 115101 (2022).

[56] A. Ataei, G. Grissonnanche, M.-E. Boulanger, L. Chen, E. Lefrancois, V. Brouet, and L. Taillefer, Impurity-induced phonon thermal Hall effect in the antiferromagnetic phase of Sr_2IrO_4, arXiv:2302.03796.

[57] J. G. Rau, E. K.- H. Lee, and H.- Y. Kee, Generic spin model for the honeycomb iridates beyond the Kitaev limit, Phys. Rev. Lett. **112**, 077204 (2014).

[58] J. Chaloupka and G. Khaliullin, Hidden symmetries of the extended Kitaev-Heisenberg model: Implications for the honeycomb-lattice iridates A_2IrO_3, Phys. Rev. B **92**, 024413 (2015).

[59] H. Liu, J. Chaloupka, and G. Khaliullin, Kitaev spin liquid in 3D transition metal compounds, Phys. Rev. Lett. **125**, 047201 (2020).

[60] T. Holstein and H. Primakoff, Field dependence of the intrinsic domain magnetization of a ferromagnet, Phys. Rev. **58**, 1098 (1940).

[61] J. H. P. Colpa, Diagonalization of the quadratic boson Hamiltonian, Physica A **93**, 327 (1978).

[62] P. A. Maksimov, Z. Zhu, S. R. White, and A. L. Chernyshev, Anisotropic-exchange magnets on a triangular lattice: Spin waves, accidental degeneracies, and dual spin liquids, Phys. Rev. X **9**, 021017 (2019).

[63] P. A. Maksimov and A. L. Chernyshev, Rethinking α-$RuCl_3$, Phys. Rev. Res. **2**, 033011 (2020).

[64] R. Matsumoto and S. Murakami, Theoretical Prediction of a rotating magnon wave packet in ferromagnets, Phys. Rev. Lett. **106**, 197202 (2011).

[65] S. Park and B.- J. Yang, Topological magnetoelastic excitations in noncollinear antiferromagnets, Phys. Rev. B **99**, 174435 (2019).

[66] X. Zhang, Y. Zhang, S. Okamoto, and D. Xiao, Thermal Hall effect induced by magnon-phonon interactions, Phys. Rev. Lett. **123**, 167202 (2019).

[67] G. Go, S. K. Kim, and K.- J. Lee, Topological Magnon-Phonon Hybrid Excitations in two-dimensional ferromagnets with tunable chern numbers, Phys. Rev. Lett. **123**, 237207 (2019).

[68] S. Park, N. Nagaosa, and B.- J. Yang, Thermal Hall effect, spin Nernst effect, and spin density induced by a thermal gradient in collinear ferrimagnets from magnon–phonon interaction, Nano Lett. **20**, 2741 (2020).

[69] B. Sheikhi, M. Kargarian, and A. Langari, Hybrid topological magnon-phonon modes in ferromagnetic honeycomb and kagome lattices, Phys. Rev. B **104**, 045139 (2021).

[70] B. Ma and G. A. Fiete, Antiferromagnetic insulators with tunable magnon-polaron Chern numbers induced by in-plane optical phonons, Phys. Rev. B **105**, L100402 (2022).

[71] C. Xu, C. Carnahan, H. Zhang, M. Sretenovic, P. Zhang, D. Xiao, and X. Ke, Thermal Hall effect in a van der Waals triangular magnet $FeCl_2$, Phys. Rev. B **107**, L060404 (2023).

[72] E. Thingstad, A. Kamra, A. Brataas, and A. Sudbø, Chiral phonon transport induced by topological magnons, Phys. Rev. Lett. **122**, 107201 (2019).

[73] N. Bazazzadeh, M. Hamdi, S. Park, A. Khavasi, S. M. Mohseni, and A. Sadeghi, Magnetoelastic coupling enabled tunability of magnon spin current generation in two-dimensional antiferromagnets, Phys. Rev. B **104**, L180402 (2021).

[74] A. Tari, *The Specific Heat of Matter at Low Temperatures* (Imperial College Press, London, 2003).